Journal of Materials Chemistry A

Accepted Manuscript

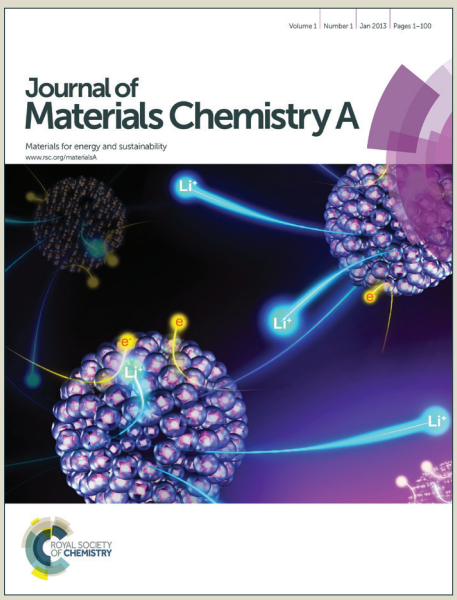

ROYAL SOCIETY OF CHEMISTRY

www.rsc.org/materialsA

Journal of Materials Chemistry A

Dynamic Article Links►

Cite this: DOI: 10.1039/c0xx00000x

PAPER

www.rsc.org/MaterialsA

High-performance lithium iron phosphate with phosphorus-doped carbon layers for lithium ion batteries

Zhang Jinli[a,b],Wang Jiao[a], Liu Yuanyuan[a], Nie Ning[a], Gu Junjie[a], Yu Feng[b] and Li Wei[a,*]

Received (in XXX, XXX) XthXXXXXXXXX 20XX, Accepted Xth XXXXXXXXX 20XX

DOI: 10.1039/b000000x

A novel composite of $LiFePO_4$ with phosphorus-doped carbon layers has been prepared via a simple hydrothermal method using glucose as the carbon source to generate the carbon coating and triphenylphosphine as the phosphorus source. Effects of phosphorus doping on the phase purity, morphology and electrochemical performance of the materials are studied by the characterizations of X-ray diffraction, Raman spectra, scanning electron microscopy, high resolution transmission electron microscopy and electrochemical techniques. It is indicated that phosphorus doping into the carbon layers is beneficial for the graphitization of the carbon. Phosphorus in the carbon layers exists in the form of P-C bond and its concentration depends on the second calcination temperature. Moreover, phosphorus-doped carbon layers on the particle surface make the charge transfer resistance decreased remarkably from 156.5 Ω to 49.1 Ω, which can be ascribed to the free carriers donated by phosphorus. The as-prepared $LiFePO_4$ with phosphorus-doped carbon layers calcined at 600 °C shows the best electrochemical performance with a discharge capacity of 124.0 mAh g^{-1} at the high rate of 20 C and an excellent retention rate of 91.4% after 50 cycles. The $LiFePO_4$ with phosphorus-doped carbon layers exhibits excellent electrochemical performances especially at high current rates, which is a promising cathode material for high-performance lithium ion batteries.

1. Introduction

Olivine structured lithium iron phosphate ($LiFePO_4$) is one of the most promising candidates for cathode materials of rechargeable lithium ion batteries applied in new energy storage devices, due to the advantages of cost reduction, environmental benignity, electrochemical and thermal stability, appropriate operating voltage and relatively high theoretical specific capacity of 170 mAh g^{-1}.[1-4] However, $LiFePO_4$ has intrinsic drawbacks including low electronic conductivity and low lithium ion diffusivity,[5-8] which have hindered its large-scale production and especially further application in electrical/hybrid vehicles. Thus, extensive efforts have been made to improve the properties of existing $LiFePO_4$-based electrode materials, including the reduction of particle size,[9-11] atomic-level doping with alien ions[12-14] and surface modification by coating with electronically conductive agents.[15-19] Among these methods, the well-known surface carbon coating is one of the most effective ways to improve the electrochemical performance of the electrode materials. However, solely through pristine carbon coating, a superior rate performance of the $LiFePO_4$ materials cannot be achieved.

Recently, nitrogen-doped carbon has been considered as a promising anode material candidate for high performance lithium ion batteries.[20-22] It is reported that doping nitrogen into the carbon layers can further enhance the electronic conductivity of the bulk since the additional electrons contributed by the nitrogen atom provide electron carriers for the conduction band.[23-25] For example, Yoon et al. prepared rod-like $LiFePO_4$ with a conductive nitrogen-doped carbon layer on the particle surface using hydrothermal method, which exhibited an initial discharge capacity of 98 mAh g^{-1} at 5 C.[26] Almost at the same time, Yang et al. prepared a hierarchical porous composite of $LiFePO_4$ with nitrogen-doped carbon nanotubes by a sol-gel method, which delivered a capacity of ~77 mAh g^{-1} at the current density at 5 C.[27] Additionally, Zhang et al. synthesized $Li_4Ti_5O_{12}$ composite with the coating of nitrogen-doped carbon layers, which showed the superior performance with the discharge capacity of 100 mAh g^{-1} at a high rate of 24 C.[28] More recently, doping phosphorus into the graphene support to improve the performance of certain catalysts for the oxygen reduction or CO oxidation reaction has been extensively studied.[29] It is reported that phosphorus doping affects the degree of graphitization and surface areas of carbon materials,[30] the doped phosphorus can modify the electron transport properties and the affinity towards acceptor molecules (such as O_2), which make phosphorus-doped carbons more efficient electrocatalysts.[31] These results enlightened us to study whether or not the phosphorus doping can accelerate the conductivity of the carbon layers and consequently improve the electrochemical performance of the battery materials.

To our knowledge, no literature has been found on the application of phosphorus-doped carbon coating on the $LiFePO_4$ surface to improve electrochemical performance of the material. In this work, we have successfully synthesized $LiFePO_4$/C through a simple hydrothermal method and incorporated phosphorus into the carbon layers by an additional calcination process using triphenylphosphine (TPP) as the phosphorus source. Effect of calcination temperature on the electrochemical properties as well as phase purity and morphology are analyzed by characterizations of X-ray diffraction (XRD), Raman spectra, X-ray photoelectron spectroscopy (XPS), scanning electron microscopy (SEM), high resolution transmission electron microscopy (HRTEM), thermogravimetric (TG) analysis and electrochemical techniques.

2. Experimental

2.1. Preparation of samples

$LiFePO_4$/C and phosphorus-doped $LiFePO_4$/C were prepared by a simple hydrothermal process using $LiOH{\cdot}H_2O$ (≥95%, Sigma-Aldrich), $FeSO_4{\cdot}7H_2O$ (AR, Sigma-Aldrich), H_3PO_4 (≥85%, Sigma-Aldrich) as starting materials, glucose (AR, Sigma-Aldrich) as the carbon source and TPP (≥99%, Sigma-Aldrich) as the phosphorus source. In the typical synthesis of $LiFePO_4$, the molar ratio of Li ∶ Fe ∶ P is 3 ∶ 1 ∶ 1 in the precursor solution, and the concentration of transition metal was controlled at 0.5 mol L^{-1}. A solution of H_3PO_4 with glucose was firstly added into a LiOH solution dropwise under vigorous stirring, immediately forming a white suspension. A degassed $FeSO_4$ aqueous solution was then slowly added into the above as-prepared white suspension under N_2 protection. Subsequently, the obtained pale green suspension was quickly transferred into an autoclave and maintained at 180 °C under mechanical stirring for 3 h. After cooling down to the room temperature, the precipitate was filtered and washed with de-ionized water three times before dried at 120 °C for 12 h under vacuum. To obtain carbon coated $LiFePO_4$ powder with well crystallized phase and good electrochemical performance, the dried samples were calcinated at 700 °C for 6 h under a N_2 flow. The obtained $LiFePO_4$/C sample was named as LFP/C. To prepare the phosphorus-doped $LiFePO_4$/C, 10mL ethanol solution with 0.2 g mL^{-1} TPP was mixed with 4 g as-prepared $LiFePO_4$/C powders, followed by the dessication at 100 °C for 10 h under vacuum and then the calcination under N_2 atmosphere for 4 h at the temperature of 300, 500, 600 or 700 °C respectively. For simplicity, the samples calcinated at different temperatures were denoted as LFP/C-P1, LFP/C-P2, LFP/C-P3 and LFP/C-P4 respectively when the temperature rose from 300 to 700 °C.

2.2. Structure and morphology characterizations

The samples were characterized by XRD (Rigaku D/MAX-2500) with a Cu *Kα* source (λ=0.154 nm) at 35 kV and 20 mA. Data were collected between 15° and 75° (2θ degree) in the step of 3° min^{-1}. Morphologies of the samples were observed via SEM images using a Hitachi S4800 microscope (INSA, Lyon). HRTEM images were recorded using a JEM100CXII instrument operating at an accelerating voltage of 100 kV. TG analysis was performed on a Netzsch-STA 449C from 25 to 700 °C at a heating rate of 10 °C min^{-1} in air. XPS measurements were performed by a PHI5000 Versa Probe spectrometer, equipped with a monochromatized Al Kα X-ray source (24.2 W) and an analyzer pass energy of 187.85 eV for survey scans. Raman spectra were obtained from a DXR microscope Raman spectrometer system equipped with a 532.4 nm laser. Specific surface areas and pore volume of the samples were determined through N_2 adsorption-desorption isotherms using Quantachrome NovaWin2 autosorb automated gas sorption system (USA). The electrical conductives were measured on San Feng SB120 using a four-point probes method.

2.3. Electrochemical characterization

Electrochemical measurements were carried out with CR2032 coin cells using metallic lithium as the anode at room temperature. Composite positive electrode was prepared by thoroughly mixing the active phosphate material, acetylene black (Shanghai Chemical Reagents Corporation) and polyvinylidene fluoride (PVDF, Shanghai Chemical Reagents Corporation) (80 ∶ 10 ∶ 10 wt.%) in N-methyl-pyrrolidinone and spread onto aluminum foils then dried for 12 h at 120 °C in vacuum. The electrolyte was a mixed solvent of ethylene carbonate (EC, Novolyte, battery grade) and dimethyl carbonate (DMC, Novolyte, battery grade) (1:1, v/v) containing 1.0 mol L^{-1} $LiPF_6$ (Sigma-Aldrich, battery grade). Coin-type cell was assembled in an argon-filled glove box with H_2O and O_2 content less than 0.1 ppm, using lithium metal as the counter electrode and Celgard 2400 as the separator. Galvanostatic charging-discharging experiments were carried out on LAND-CT2001A (Wuhan Kingnuo Electronic Co.) in the cut-off voltages of 2.2 and 4.2 V versus Li/Li^+ at room temperature. The electrochemical impedance spectroscopic analysis (EIS) was carried out with CHI604D (CH Instruments, China) by applying a 5 mV amplitude signal over the frequency range between 100 kHz and 0.1Hz.

3. Results and discussion

The phase compositions of the as-prepared samples were determined by XRD patterns. As shown in Fig. 1, all the obtained

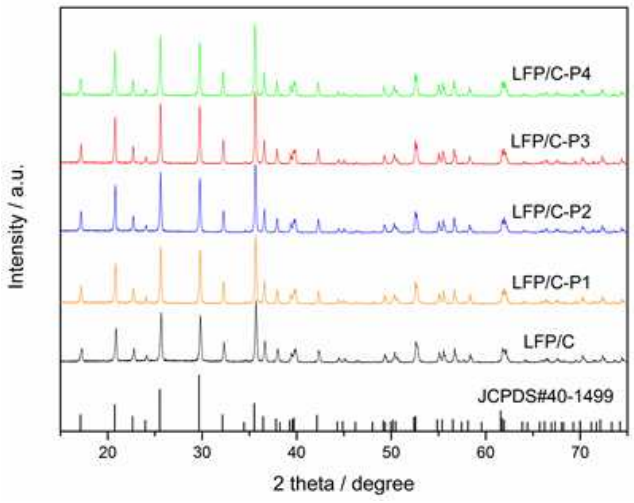

Fig. 1. XRD patterns of LFP/C and LFP/C-P.

samples show strong and narrow diffraction peaks, which can be indexed to an orthorhombic structure with a space group of Pnma (JCPDS card NO.40-1499). It is worth noting that no diffraction

peak indicative of a second phase is found, indicating the high crystallinity and phase purity of all the $LiFePO_4$ samples. Obviously, the incorporation of phosphorus into the carbon layers has no effect on the formation of crystalline structure of $LiFePO_4$. It is suggested that well crystallized LFP/C-P samples without any impurity phase can be prepared at the calcination temperature ranged from 300 to 700 °C.

Raman spectra were measured to investigate the density of defects at the sample surfaces. As shown in Fig. 2, the peaks near 1325 and 1592 cm^{-1} are assigned to D-band and G-band, respectively. The G-band is associated with the vibration of sp^2-bonded carbon atoms in a 2D hexagonal lattice, while the D-band corresponds to the defect-induced mode.[32] These two peaks can be detected in all of the five samples, suggesting that a carbon film is successfully coated onto the surface of each sample. Generally, it is considered that the graphite carbon on the surface of the materials shows higher conductivity compared with disorder carbon and thus enhances the electronic conductivity during the charge/discharge process,[33] i.e., the larger amount of graphite carbon on the surface, the better electrochemical properties of the materials. The intensity ratio of D and G bands (I_D/I_G) is used to evaluate the degree of graphitization of the carbon layers on the surface of the materials. As listed in Table 1,

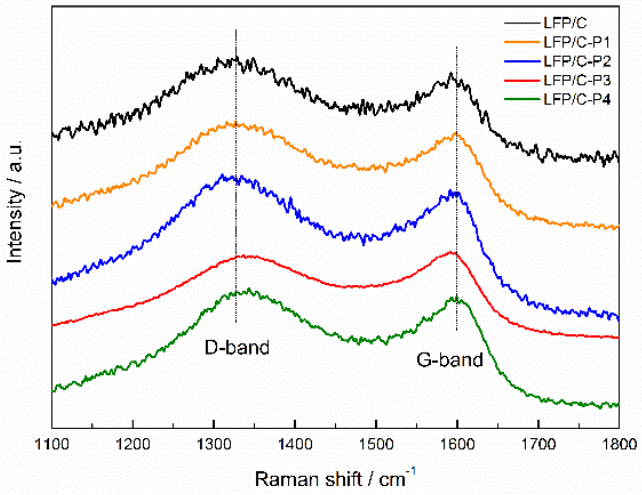

Fig. 2. Raman spectrum of LFP/C and LFP/C-P.

Table 1 I_D/I_G of LFP/C and LFP/C-P materials.

Sample	I_D/I_G
LFP/C	1.38
LFP/C-P1	1.19
LFP/C-P2	1.17
LFP/C-P3	0.96
LFP/C-P4	1.11

the carbon layers of the phosphorus-doped samples show a relatively lower I_D/I_G ratio, indicating the positive effect of phosphorus doping on the graphitization of the carbon layers, compared with sample LFP/C. Obviously, the sample LFP/C-P3, with an I_D/I_G ratio of 0.96, exhibits the highest degree of graphitization, which is probably responsible for the excellent electrochemical performance of the sample, as discussed in the next context.

XPS spectra of LFP/C-P samples were analyzed to determine the composition content and the species of phosphorus in the carbon layers. As listed in Table 2, the LFP/C sample without phosphorus doping consists of 41.73 % carbon and 3.92 % phosphorus, with the P:C ratio of 0.09. For the sample with phosphorus doping, the relative ratio of P:C is increased and achieves the highest of 0.13 for LFP/C-P3. The phosphorus species were discriminated through the deconvolution of XPS P 2p profiles for these samples.

Table 2 The composition contents and relative ratios in the carbon layers of LFP/C and LFP/C-P materials

Sample	atm.%			P:C	P:O
	P	C	O		
LFP/C	3.92	41.73	15.89	0.09	0.25
LFP/C-P1	4.13	40.76	16.20	0.10	0.25
LFP/C-P2	4.35	39.50	17.31	0.11	0.25
LFP/C-P3	4.70	35.33	18.98	0.13	0.25
LFP/C-P4	4.68	43.14	18.39	0.11	0.25

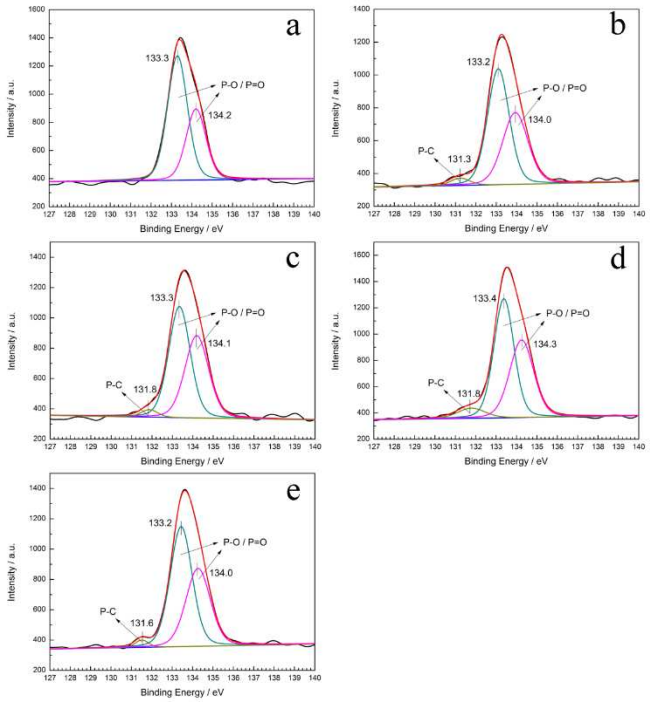

Fig. 3. XPS spectra of P 2p of (a) LFP/C, (b) LFP/C-P1, (c) LFP/C-P2, (d) LFP/C-P3 and (e) LFP/C-P4.

As shown in Fig. 3a, the undoped LFP/C exhibits two peaks at 133.3 and 134.2 eV, which are respectively corresponding to P-O and P=O.[34,35] For LFP/C-P samples there appears a new small peak at 131.6±0.3 eV, attributing to the bonding of P-C (Fig. 3b - 3e).[35] As listed in Table 3, the P-C content of LFP/C-P samples increases from 3.1% to 8.1% as the calcination temperature rises from 300 °C to 600 °C, suggesting that the higher calcination temperature is beneficial to the formation of P-C chemical bondings in the carbon layers around $LiFePO_4$. The P-C content of LFP/C-P3 equals the maximum of 8.1%, whereas for the LFP/C-P4 sample the P-C content is as low as 3.1%, which is probably due to the sublimation of elemental phosphorus in the carbon layers at the temperature higher than 600 °C.[36]

Table 3 The relative content of phosphorous species in XPS spectra of LFP/C and LFP/C-P materials.

Sample	Binding energy / eV			Peak area ratio / %		
	P-C	P-O / P=O		P-C	P-O / P=O	
LFP/C		133.3	134.2		63.7	36.3
LFP/C-P1	131.3	133.2	134.0	3.1	56.2	40.7
LFP/C-P2	131.8	133.3	134.1	3.4	56.3	40.3
LFP/C-P3	131.8	133.4	134.3	8.1	56.4	35.5
LFP/C-P4	131.6	133.5	134.3	3.1	56.8	40.1

Morphologies of all the $LiFePO_4$ samples were detected by SEM and HRTEM. SEM images indicate that for the undoped LFP/C or the phosphorus doped LFP/C-P there are rod-like particles with a length distribution from 200 to 300 nm and a width ranging from 100 to 200 nm (Fig. 4a - 4e). HRTEM images show that both LFP/C and LFP/C-P samples are coated by thin carbon layers with the thickness about 4 nm (Fig. 4f - 4j). To confirm the carbon content of all the five samples, the TG analysis was performed. Based on the difference in the TG weight gain observed in $LiFePO_4$ and the five different samples, the carbon content of LFP/C, LFP/C-P1, LFP/C-P2, LFP/C-P3 and LFP/C-P4 is 1.9 wt%, 2.0 wt%, 1.9 wt%, 2.0 wt% and 1.9 wt%, respectively.[37] It is suggested that the calcination process for phosphorus doping has no significantly influence on the morphology and the carbon coatings of $LiFePO_4$ materials.

Table 4 lists the specific surface area and the pore volume of the undoped LFP/C or the phosphorus doped LFP/C-P samples. It is clear that LFP/C-P3 has the largest specific surface area of 27.08 $m^2 g^{-1}$, increased by 44% compared with that of LFP/C (18.85 $m^2 g^{-1}$), meanwhile the pore volume of LFP/C-P3 is 0.010 cc g^{-1}, which is increased by 43% compared with that of LFP/C (0.007 cc g^{-1}). Whereas for the LFP/C-P4 sample that experienced the calcination at 700 °C the specific surface area and the pore volume decrease greatly. It is illustrated that the calcination process for phosphorus doping with temperature lower than 600 °C can increase both the specific surface area and pore volume of the carbon layers around $LiFePO_4$ materials, which is beneficial to quick migrations of lithium ions and

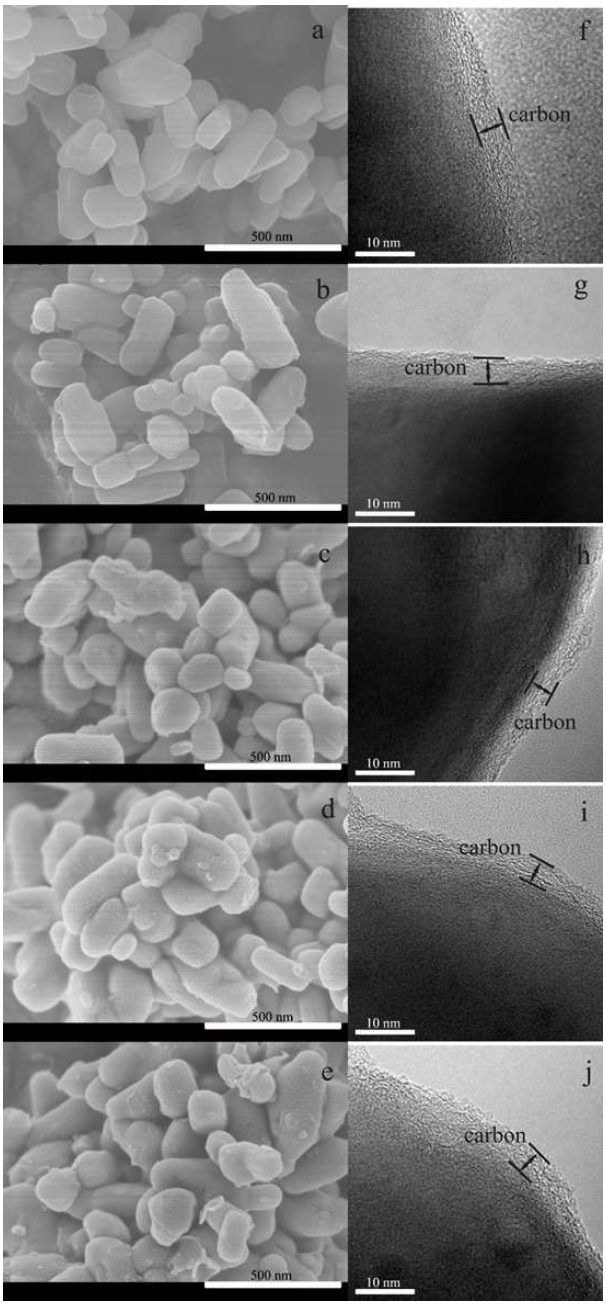

Fig. 4. SEM and HRTEM images of (a, f) LFP/C, (b, g) LFP/C-P1, (c, h) LFP/C-P2, (d, i) LFP/C-P3 and (e, j) LFP/C-P4.

Table 4 Specific structure parameters of LFP/C and LFP/C-P materials.

Sample	specific surface area / $m^2 g^{-1}$	pore volume / cc g^{-1}
LFP/C	18.85	0.007
LFP/C-P1	24.77	0.009
LFP/C-P2	21.30	0.008
LFP/C-P3	27.08	0.010
LFP/C-P4	19.71	0.007

consequently improves the electrochemical performance of $LiFePO_4$/C materials.

From the measurements using a four-point probes method, the electrical conductives of LFP/C, LFP/C-P1, LFP/C-P2, LFP/C-P3, LFP/C-P4 are 2.21×10^{-2}, 3.14×10^{-2}, 4.00×10^{-2}, 8.39×10^{-2} and 7.50×10^{-2} S cm^{-1} respectively, clearly indicating that the electrical conductivities are remarkably enhanced by phosphorus doping.

Fig. 5 shows the electrochemical performances of the five $LiFePO_4$ samples. The charge-discharge profiles of the five different samples at 0.1 C are shown in Fig. 5a. The initial charge/discharge profiles of all the five samples exhibit a flat voltage plateau at around 3.4 V (versus Li^+/Li), which results from the two-phase redox reaction between $FePO_4$ and $LiFePO_4$.[38,39] Generally, materials with higher platform capacity and utilization efficiency can provide longer working time for the electronic devices. In the initial cycle at the rate of 0.1 C, the discharge capacities of LFP/C, LFP/C-P1, LFP/C-P2, LFP/C-P3, LFP/C-P4 at 0.1C are 152.8, 158.4, 164.1, 165.5 and 164.2 mAh g^{-1} respectively and the coulombic efficiency are 98%, 98%, 98%, 99% and 99% respectively. The LFP/C-P3 sample shows the highest platform capacity, indicating that the phosphorus doping into the carbon layers of $LiFePO_4$ particles can elevate the specific capacities but also the coulombic efficiency of $LiFePO_4$ materials. Fig. 5b compares the rate performances of the undoped LFP/C and the phosphorus doped LFP/C-P samples at different current densities from 0.1 to 20 C. Under various charge/discharge rates, the phosphorus-doped LFP/C-P samples show significant higher capacities than the undoped LFP/C sample, especially the LFP/C-P3 sample exhibits the highest discharge capacities at various rates. It is indicated that there is less polarization inside the electrode for the phosphorus-doped samples, and the advantage becomes even apparent as the charge/discharge rates increases. Fig. 5c displays the cycling performance of the LFP/C-P3 sample and the undoped LFP/C at 20 C. The corresponding specific discharge capacities of sample LFP/C and LFP/C-P3 are 105.4 and 124.0 mAh g^{-1} in the initial cycle, and decreases to 90.7 and 113.3 mAh g^{-1} after 50 charge/discharge cycles, keeping 86.1% and 91.4% retention of the initial capacities, respectively. Obviously, the phosphorus doped LFP/C-P3 exhibits significant higher discharge capacities than that of the undoped LFP/C, suggesting that phosphorus doping into the carbon layers not only improves the specific capacities at various rates, but also elevates the cycling performance of the materials.

These extraordinary electrochemical performances of the phosphorus-doped $LiFePO_4$/C materials reveal that the phosphorus-doped carbon layers can construct the pathways for effective transferring of the electrons even under high charge/discharge rates. It is attributed to the good electron-donor properties of phosphorus. Plenty of free carriers provided by phosphorus may increase the conductivity of the $LiFePO_4$/C samples so as to improve the electrochemical performance of the materials, which is confirmed by the above results showing that sample LFP/C-P3 with the highest content of P-C bonds exhibits the best electrochemical performance. Moreover the migration rate of lithium ions and the mass transfer rate can be improved because of the largest surface area and pore volume of sample LFP/C-P3. All of these reasons together make a significant contribution to the improvement of electrochemical performances of the phosphorus-doped sample LFP/C-P3.

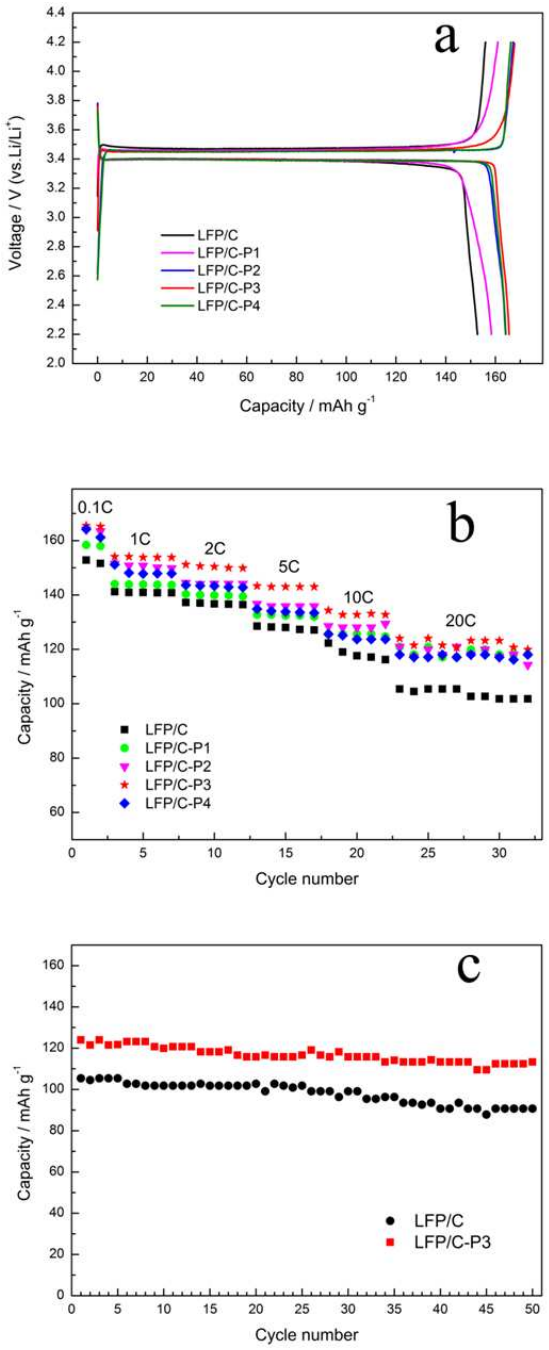

Fig. 5. (a) The charge-discharge profiles of LFP/C and LFP/C-P at 0.1 C; (b) the multi-rate capability of LFP/C and LFP/C-P; (c) the cycleperformance of LFP/C and LFP/C-P3 at 20 C.

EIS measurement was carried out to deeply understand the effect of phosphorus doping on the electrochemical properties. The EIS datas were analyzed based on the equivalent circuit shown in Fig. 6a, where R_u refers to uncompensated resistance that includes a number of contributions: particle-particle contact resistance, electrolyte resistance, and the resistance between the electrode and the current collector. R_{ct} refers to charge transfer resistance which is related to the electrochemical reaction at the electrode-electrolyte interface and particle-particle contact. CPE

represents the dispersion effects caused by the inhomogeneity such as the impurity and the defects in the crystals. R_u and CPE are unaffected by the phosphorus doping.[28,40,41] Fig. 6b shows the EIS spectra of LFP/C and LFP/C-P3. The abscissa axis and the ordinate axis represent the real part and the imaginary part of the resistance respectively. The semicircle in the high and middle frequency regions is resulted from the charge transfer resistance. While the sloping line in the lower frequency represents the Warburg impedance (Z_w), which is associated with lithium ions diffusion in the bulk of the electrode.[26] Obviously, the diameter of the semicircle of LFP/C-P3 is smaller than that of LFP/C from the Nyquist plot. As a result, the charge transfer resistance decreases from 156.5 Ω in LFP/C to 49.1 Ω in LFP/C-P3. That is to say, the increase of free charge carriers donated by phosphorus can be directly reflected from the decrease of the specific resistivity. The reduction of the charge transfer impedance is beneficial to overcome the dynamic limitations of the process, so as to improve the electrochemical properties. Moreover, the slope of the line of LFP/C-P3 is higher than that of LFP/C, indicating that the Warburg impedance (Z_w) of LFP/C-P3 decreases as well. The exchange current density (i_0) is a very important parameter of kinetics for an electrochemical reaction, and can measure the catalytic activity of electrodes. It is calculated using the following formula:

$$i_0 = \frac{RT}{nFR_{ct}} \quad (1)$$

where R is the gas constant (8.314 J mol^{-1} K^{-1}), T is the temperature (298 K), n is the charge transfer number per molecule during the intercalation, and F is the Faraday's constant (96500 C mol^{-1}).[42] The i_0 value of LFP/C-P3 (0.5 mA) is higher than that of LFP/C (0.2 mA), which is in accordance with its excellent electrochemical performances, displayed in Fig. 5. The lithium ion diffusion coefficients (D) are calculated according to the following equation:

$$D = \frac{R^2T^2}{2A^2n^4F^4C^2\sigma^2} \quad (2)$$

where R is the gas constant, T is the absolute temperature, A is the surface area of the cathode, n is the number of electrons per molecule during oxidization, F is the Faraday constant, C is the concentration of lithium ion, and σ is the Warburg factor which is relative with Z':

$$Z' = R_D + R_L + \sigma\omega^{-\frac{1}{2}} \quad (3)$$

Fig. 6c shows the relationship between Z' and reciprocal square root of frequency ($\omega^{-1/2}$) in the low-frequency region. The calculated lithium ion diffusion coefficients of LFP/C and LFP/C-P3 are 1.15×10^{-13} and 1.72×10^{-13} cm^2 s^{-1}, respectively, suggesting that the phosphorus-doped sample LFP/C-P3 is more mobile for diffusions of lithium ions and thus has better electrochemical performance than undoped LFP/C.[43] Therefore, the EIS analysis further confirms that phosphorus-doping carbon coating is effective to improve the electrical conductivity of $LiFePO_4$.

4. Conclusions

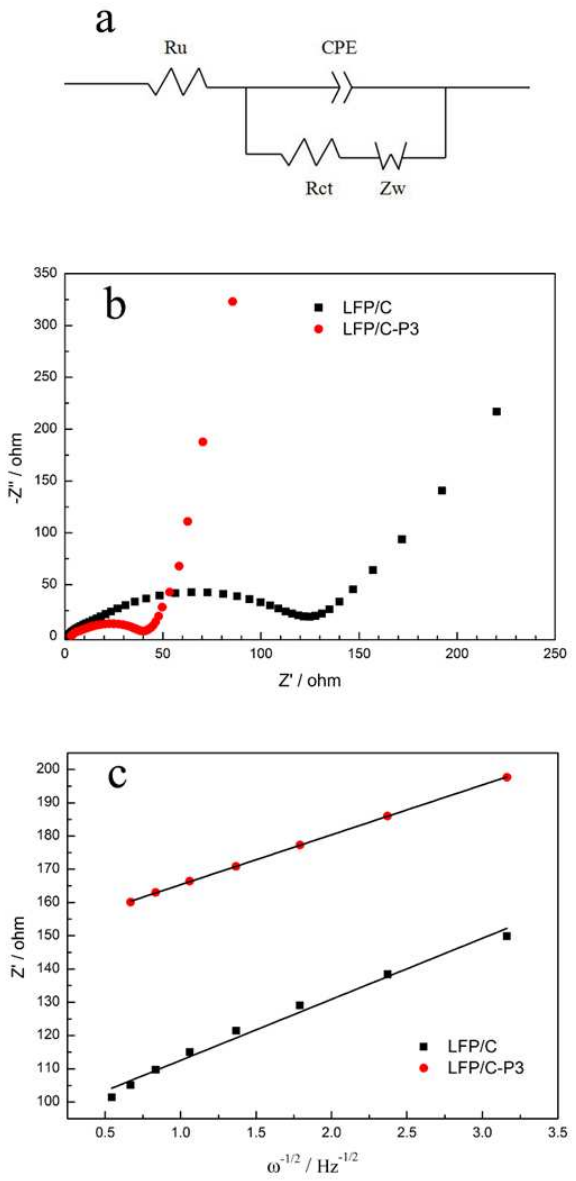

Fig. 6. (a) Equivalent circuit model; (b) EIS of LFP/C and LFP/C-P3; (c) the relationship between Z' and reciprocal square root of frequency ($\omega^{-1/2}$).

We have successfully synthesized phosphorus-doped $LiFePO_4$/C materials via a simple hydrothermal method at various calcination temperatures. The P-C concentration of the phosphorus-doped carbon layers changes with calcination temperatures and reaches a maximum at 600 °C, under which conditions the prepared $LiFePO_4$/C-P exhibits the best electrochemical performances. In comparison with undoped $LiFePO_4$/C, the electron-donating phosphorus-doped $LiFePO_4$/C-P shows higher specific capacities and better rate performances with relatively lower charge transfer resistance which may be ascribed to a higher concentration of free charge carriers. The phosphorus-doped $LiFePO_4$/C materials are rather promising for high power lithium ion batteries. Such a novel strategy with its facile preparation process may be extended to the preparations of other cathode materials for advanced batteries applied in electric vehicles.

Acknowledgements

This work is financially supported by the Special Funds for Major State Basic Research Program of China (2012CB720300), NSFC (21476158), and Program for Changjiang Scholars and Innovative Research Team in University (IRT1161).

Notes and references

a School of Chemical Engineering, Tianjin University, Tianjin300072, China. Fax: 86-22-27890643; Tel: 86-22-27890643; E-mail: liwei@tju.edu.cn

b School of Chemical Engineering, Shihezi University, Shihezi832003, China.

† Electronic Supplementary Information (ESI) available: [details of any supplementary information available should be included here]. See DOI: 10.1039/b000000x/

1 S. Nishimura, G. Kobayashi, K. Ohoyama, R. Kanno, M. Yashima and A. Yamada, Nat. Mater., 2008, **7**, 707.
2 K. Padhi A, S. Nanjundaswamy K and B. Goodenough J, J. Electrochem. Soc.,1997, **144**, 1188.
3 J.M. Tarascon and M. Armand, Nature, 2001, **414**, 359.
4 J. Wang and X. Sun, Energy Environ. Sci., 2012, **5**, 5163.
5 A.S. Andersson, J.O. Thomas, B. Kalska and L. Haggstrom, Electrochem. Solid-State Lett., 2000, **3**, 66.
6 S.Y. Chung and Y.M. Chiang, Electrochem. Solid-State Lett., 2003, **6**, A278.
7 C. Delacourt, L. Laffont, R. Bouchet, C. Wurm, J.B. Leriche, M. Morcrette, J.M. Tarascon and C. Masquelier, J. Electrochem. Soc., 2005, **152**, A913.
8 A. Yamada, Y. Takei, H. Koizumi, N. Sonoyama, R. Kanno, K. Itoh, M. Yonemura and T. Kamiyama, Chem. Mater., 2006, **18**, 804.
9 B. Kang and G. Ceder, Nature, 2009, **458**, 190.
10 A.V. Murugan, T. Muraliganth and A. Manthiram, Electrochem. Commun., 2008, **10**, 903.
11 K. Saravanan, P. Balaya, M.V. Reddy, B.V.R. Chowdari and J.J. Vittal, Energy Environ. Sci., 2010, **3**, 457.
12 S.Y. Chung, J.T. Bloking and Y.M. Chiang, Nat. Mater., 2002, **1**, 123.
13 K.L. Harrison and A. Manthiram, Inorg. Chem., 2011, **50**, 3613.
14 P.S. Herle, B. Ellis, N. Coombs and L.F. Nazar, Nat. Mater., 2004, **3**, 147.
15 R. Dominko, M. Gaberscek, J. Drofenik, M. Bele, S. Pejovnik and J. Jamnik, J. Power Sources, 2003, **119**, 770.
16 A.V. Murugan, T. Muraliganth and A. Manthiram,J. Electrochem. Soc., 2009, **156**, A79.
17 S.W. Oh, S.T. Myung, S.M. Oh, K.H. Oh, K. Amine, B. Scrosati and Y.K. Sun, Adv. Mater., 2010, **22**, 4842.
18 N. Ravet, Y. Chouinard, J.F. Magnan, S. Besner, M. Gauthier and M. Armand, J. Power Sources, 2001, **97-8**, 503.
19 G.M. Song, Y. Wu, Q. Xu and G. Liu, J. Power Sources, 2010, **195**, 3913.
20 C. Ma, X. Shao and D. Cao, J. Mater. Chem., 2012, **22**, 8911.
21 Y.P. Wu, C.Y. Jiang, C.R. Wang, S.B. Fang and Y.Y. Jiang, J. Appl. Polym. Sci., 2000, **77**, 1735.
22 Z. Zhou, X.P. Gao, J. Yan, D.Y. Song and M. Morinaga, Carbon, 2004, **42**, 2677.
23 S. Chen, J.J. Duan, M. Jaroniec and S.Z. Qiao, Adv. Mater., 2014, **26**, 2925.
24 L. Qie, W.M. Chen, Z.H. Wang, Q.G. Shao, X. Li, L.X. Yuan, X.L. Hu, W.X. Zhang and Y.H. Huang, Adv. Mater., 2012, **24**, 2047.
25 J.J. Duan, Y. Zheng, S. Chen, Y.H. Tang, M. Jaroniec and S.Z. Qiao, Chem Commun., 2013, **49**,7705.
26 S. Yoon, C. Liao, X.G. Sun, C.A. Bridges, R.R. Unocic, J. Nanda, S. Dai and M.P. Paranthaman, J. Mater. Chem., 2012, **22**, 4611.
27 J. Yang, J. Wang, X. Li, D. Wang, J. Liu, G. Liang, M. Gauthier, Y. Li, D. Geng, R. Li and X. Sun, J. Mater. Chem., 2012, **22**, 7537.
28 H. Zhang, Q. Deng, C. Mou, Z. Huang, Y. Wang, A. Zhou and J. Li, J. Power Sources, 2013, **239**, 538.
29 Z. Mo, S. Liao, Y. Zheng and Z. Fu, Carbon, 2012, **50**, 2620.
30 Z.W. Liu, F. Peng, H.J. Wang, H. Yu, W.X. Zheng and J. Yang, Angew. Chem. Int. Ed., 2011, **50**, 3257.
31 J. Wu, Z.R. Yang, X.W. Li, Q.J. Sun, C. Jin, P. Strasser and R.Z. Yang, J. Mater. Chem., 2013, **A 1**, 9889.
32 Z. Wang, X. Xiong, L. Qie and Y. Huang, Electrochim. Acta., 2013, **106**, 320.
33 Y. Xia, W. Zhang, H. Huang, Y. Gan, Z. Xiao, L. Qian and X. Tao, J. Mater. Chem., 2011, **21**, 6498.
34 E. Yoo and H. Zhou, RSC Advances, 2014, **4**, 13119.
35 Y.H. Cao, H. Yu, J. Tan, F. Peng, H.J. Wang, J. Li, W.X. Zheng and N.B. Wong, Carbon, 2013, **57**, 433.
36 C. Wang, L. Sun, Y. Zhou, P. Wan, X. Zhang and J. Qiu, Carbon, 2013, **59**, 537.
37 I. Belharouak, C. Johnson, K. Amine, Electrochem. Commun., 2005, **7**, 983.
38 Y. Xia, W. Zhang, H. Huang, Y. Gan, Z. Xiao, L. Qian and X. Tao, J. Mater. Chem., 2011, **21**, 6498.
39 J. Zhao, J. He, J. Zhou, Y. Guo, T. Wang, S. Wu, X. Ding, R. Huang and H. Xue, J. Phys. Chem. C, 2011, **115**, 2888.
40 C.Y. Lee, H.M. Tsai, H.J. Chuang, S.Y. Li, P. Lin and T.Y. Tseng, J. Electrochem. Soc., 2005, **152**, A716.
41 H.C. Shin, W.I. Cho and H. Jang, Electrochim. Acta., 2006, **52**, 1472.
42 J. Song, G. Shao, M. Shi, Z. Ma, W. Song, C. Wang and S. Liu, Solid State Ionics, 2013, **253**, 39.
43 H. Liu, P. Zhang, G.C. Li, Q. Wu and Y.P. Wu, J. Solid State Electrochem., 2008, **12**, 1011.